Frontier Exploration using a Towed Streamer EM system – Barents Sea Examples

Anwar Bhuiyan, Eivind Vesterås and Allan McKay, PGS Geophysical AS*

Summary

The measured Towed Streamer EM data from a survey in the Barents Sea, undertaken in the Norwegian sector are inverted as a series of unconstrained and seismically guided 2.5D inversions. The subsurface geology is complex and provides a good test area in terms of controlled source electromagnetic (CSEM) surveying. Subsurface interpretation in such a complex geological setting is a challenge due to solution ambiguities while using a single geophysical method. The integration of seismic and CSEM data, where seismic provides a high-resolution structural image and CSEM estimates the resistivity, is a more powerful tool for subsurface interpretation than either technique alone. In this paper we present both unconstrained and seismically guided inversions and illustrate how data integration improves the subsurface interpretation. Such an integrated approach can be a powerful tool in a frontier exploration setting where CSEM and seismic data co-exist. We also show how dense in-line sampling of the electric field improves the sensitivity to changes in sub-surface resistivity.

Introduction

The Norwegian Sector of the Barents Sea has experienced an increase in exploration activity over the course of the past ten or so years. CSEM data have proven to be a valuable pre-drill de-risking and prospect identification tool when used together with seismic data. Nevertheless, the Barents Sea is relatively under-explored, encompasses complex geological settings with relatively high and variable background resistivity, and anisotropic sediments.

As part of a larger acquisition campaign in 2013 PGS acquired high quality CSEM data, using a Towed Streamer EM system, in the Barents Sea; see Figure 1 for location and coverage of the acquisition.

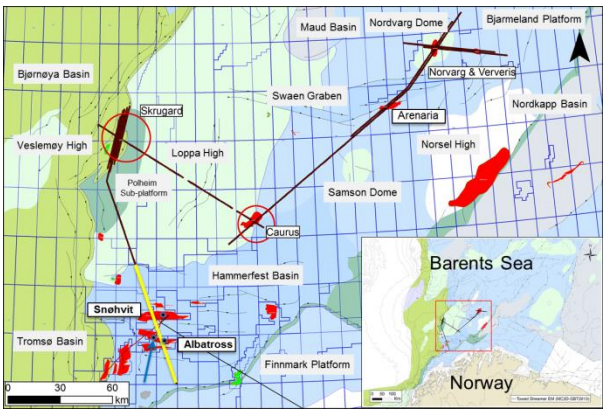

Figure 1: Location of data presented in this paper in yellow, overlaid on full coverage in black. Black stars show the well locations; the blue arrowhead indicates the well-7120/9-1 for which the measured resistivity has been compared to the EM inverted ones.

Even in a complex geological setting we show that it is possible to recover resistivity depth trends, the average interval resistivity, and interpretable resistivity sections, using unconstrained inversion. Inverted resistivities are compared to publically available well-log and dual-sensor towed streamer seismic data from the Snøhvit and Albatross areas. The integration of seismic and EM data provide a powerful tool which enables the strengths of each data type to be fully exploited. Du and Hosseinzadeh (2014) developed a workflow to make the inversion-based EM and seismic integration process more data and information-driven and less *a priori* model-driven. We show how the unconstrained inversion results can be improved further by including seismic structural constraints. In addition, we highlight how the integration of broadband dual sensor seismic data and resistivity from Towed Streamer EM can be used to identify prospective structures, in this case a stratigraphic sand lens at about 2 km depth.

One of the benefits of the Towed Steamer EM system is dense spatial sampling of the electric field. We show that high data density increases the sensitivity to prospective structures at depth, and therefore improved resistivity models.

Acquisition System

The Towed Streamer EM system consists of a single vessel towing an 800 m long Horizontal Electric Di-pole (HED) towed at 10 m, and an EM streamer that towed at 100 m depth. The streamer has 72 electric field channels, or electrode pairs, providing offsets from ~0-7708 m relative to the center of the source. The source transmits an optimized repeated sequence (ORS) generated by an oscillating current of +/- 1500 Amperes, typically over a frequency range of two decades (0.1-10 Hz). Having a shot cycle of 120 seconds and an acquisition speed of 4-5 knots the average shot distance is between 240 and 300 m.

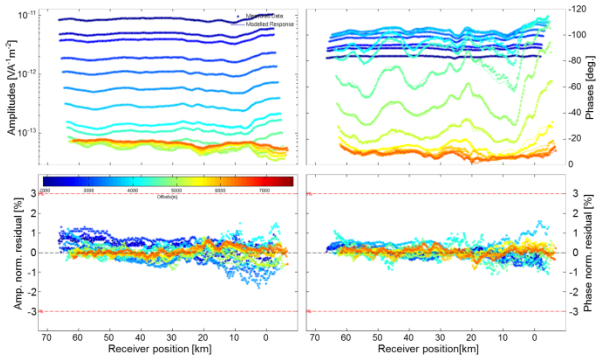

Figure 2: Subset of frequency response amplitudes (left) and phases (right) at 0.6 Hz for offsets, 1943 – 7708 m plotted along receiver positions with respect to 1st shot. Dots are data-points and solid line is model-fit. Amplitude and phase normalized RMS misfits (%) are given in the lower panels (unconstrained inversion example).

DOI http://dx.doi.org/10.1190/segam2015-5860124.1

The on-board processing consists of de-convolving the measured electric field with the output source current to obtain the frequency responses for all available offsets, frequencies and shot points, and application of noise reduction algorithms (Mattsson et al., 2012). Processed data along a survey line over Snøhvit and Albatross area shown as an example in Figure 2. The data are presented as the amplitude (upper panel, left) and phase (upper panel, right) over a selection of offsets (1943-7708 m) and a frequency of 0.6 Hz. The data quality is good with stable amplitude and phase estimates over a broad frequency and offset range (overall total uncertainties of the data are <3%). The largest uncertainty is associated with the lowest frequency and the furthest offsets (Mattson et al., 2012).

Unconstrained inversion and the sub-surface resistivity

Firstly, we undertook unconstrained anisotropic 2.5D inversion using the MARE2DEM code developed by the Scripps Seafloor Electromagnetic Consortium to recover the sub-surface resistivity. The forward modelling kernel is based on the adaptive finite element code of Key and Ovall (2011); the inversion scheme is based on smooth 'Occam' inversion (Constable et al., 1987), a regularized variant of Gauss-Newton minimization. To adequately describe the earth model we have found that an anisotropic model is needed.

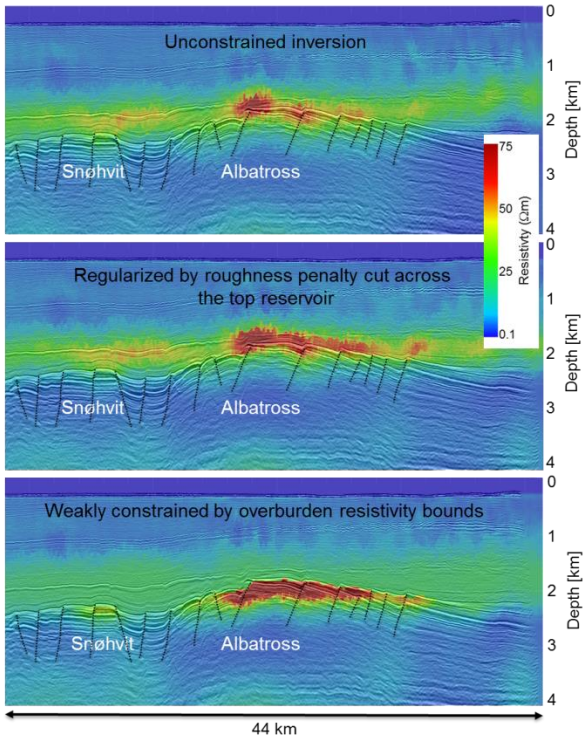

Figure 3: Figure showing unconstrained (upper panel) versus seismically guided inversion results (middle and lower panels). The middle panel represents the constrained inversion regularized by roughness penalty (0.1) along the seismic boundary (top reservoir), while the lower panel shows the seismically guided inversion (resistivity bounds, 0.5 – 25 Ωm above top reservoir). Note all inversion results include the vertical resistivity sections (horizontal resistivity sections are not shown for brevity).

We select multiple frequency and offsets covering frequencies 0.2:0.2:1 Hz, and 19 offsets in the range 1943 to 7708 m. For the unconstrained approach the inversion is initiated from a half space. The only fixed resistivity model parameters are the water resistivity (0.28 Ωm) and water depth (300 -325 m). The water depth is fixed on the basis of the measured echo-sounder data, and the resistivity is fixed based on CTD-profiles taken during the survey. About 10-20 inversion iterations are usually sufficient to reach the prescribed target misfit. In Figure 2 we show an example of the data-fit (amplitude misfit less than 3%) for the parameterization implemented in unconstrained EM data inversion.

In Figure 3 (upper panel) we show the vertical resistivity section in the vicinity of both the Snøhvit and Albatross structures. The Albatross case indicates that even in relatively complex geological settings then unconstrained inversion can produce sub-surface resistivity sections that are structurally conformant, and consistent with the logged resistivity depth trend. Here, the unconstrained inversion has reasonably recovered the resistive structure (HC charged) since it has the largest impact on the data responses, but the resistive anomalies are placed slightly too shallow.

Now we investigate how seismic data may help to locate the appropriate intervals of the potential resistivity contrasts and thus, improve the resolution of the inverted resistivity models.

Seismically guided inversion and the sub-surface resistivity

In this approach, the inversions are guided by the seismic data to find the stratigraphic boundaries, whereas the resistivity variations within the overburden are guided by plausible boundaries suggested by the unconstrained inversions. We interpret both the seismic and EM data together by matching the stratigraphic and resistivity intervals recovered from inversion. We picked only the top reservoir horizon, the top Stø Formation in this case, from the post-stack dual-sensor seismic data. The anisotropic resistivity variations within the layers above this boundary are guided by the lower and upper bounds placed on the resistivity (0.5 – 25 Ωm). The remaining regions are all set as free parameters. The seismic boundaries adopted here only for the purpose of 'guiding' the EM inversion that the geological interfaces mapped by seismic data may also be potential EM boundaries. For a detailed description of the workflow see Du and Hosseinzadeh (2014).

The guided inversion shown in the middle panel of Figure 3 is an attempt to relax the inversion smoothness condition to enable resistivity variations to follow the seismic boundary, the top reservoir in this case. The lateral resolution slightly improved, however the vertical placement remained the same compared to unconstrained inversion.

In the lower panel of Figure 3 the seismically guided inversion results are shown. In contrary to unconstrained approach, the seismically guided inversion reveals a more clearly defined anomaly within the Albatross structure coinciding reasonably well with the position of the main reservoir structures obtained from seismic data interpretation.

DOI http://dx.doi.org/10.1190/segam2015-5860124.1

The joint analysis of Towed Streamer EM and broadband dual sensor seismic data can reveal prospective structures. For example, Figure 4 shows a resistivity anomaly at ~2 km depth below sea level located ~12-15 km NW to the Snøhvit structure. This resistivity anomaly corresponds fairly well with seismically interpreted intra-Cretaceous sand lens (Figure 4, lower panel). Of course further study is needed to improve the recovered anomaly and explore the possibility that it may be prospective.

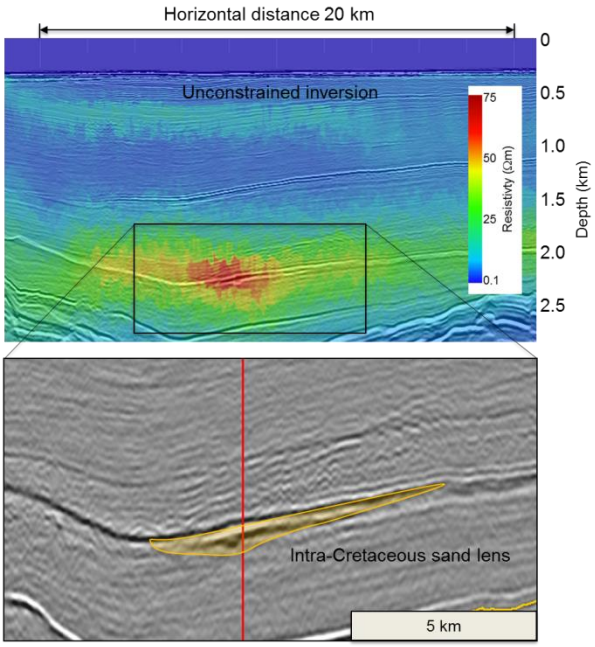

Figure 4: Resistivity anomaly recovered by unconstrained inversion (upper panel) corresponds to intra-Cretaceous sand lens (lower panel).

Figure 5 (left panel) shows the logged resistivity from the 7120/9-1 well, and the horizontal and vertical resistivity recovered using unconstrained inversion. It is evident that the horizontal resistivity is close to the logged resistivity depth trend. The vertical resistivity indicates background (over-burden) anisotropy of about 2-3. At the reservoir level then there is an increase of both the horizontal and vertical resistivity, but the largest increase is in the vertical component of resistivity. However, the unconstrained inversion recovers the high-resistivity anomaly at a shallower burial depth compared to the actual reservoir.

The overall resistivity trend observed in the well-log has been recovered fairly well in the seismically guided inverted data (Figure 5, right panel). A high resistivity anomaly has been recovered at depths of 1850–2000 m below sea level which corresponds to the Albatross discovery. A reasonable data-fit between inverted and well-log resistivities has been observed at the reservoir (vertical resistivity). The inverted resistivity in the overburden is higher compared to well-log data. Inverted horizontal resistivity at the reservoir is low compared to the log data, since the electric field mode is mainly vertical within a thin resistive layer (Løseth and Ursin, 2007). Therefore, a significant variation between the vertical and horizontal resistivity has been recovered at the reservoir level (Figure 5).

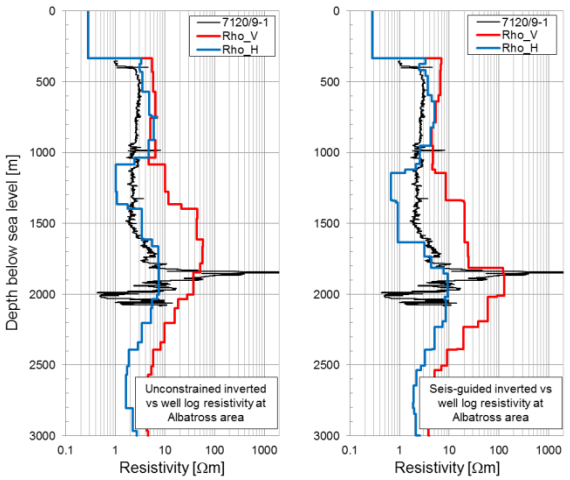

Figure 5: Comparison of measured resistivity at one well (7120/9-1) in the Barents Sea and the resistivity recovered via unconstrained (left) and seismically guided (right) anisotropic inversion.

The inversion workflow here is purely data driven, and it offers the potential to improve the resolution of the sub-surface resistivity model. We believe that it could be applied in a frontier exploration setting given both seismic and EM data are available. Of course, well logs could be used to ensure that horizons are registered in depth as accurately as possible.

Benefits of high data density

The CSEM data help interpreting sub-surface resistivity distribution provided that the inverted model is adequately robust. The Towed Streamer EM acquisition provides exceptionally dense data (with a shot spacing of 250 m, and up to 72 electric field channels). In this section, we illustrate how the dense in-line spatial sampling provides the resistivity models with improved resolution in comparison to those derived from a coarser data sampling.

First, we invert the dense data case with a 250 m in-line shot spacing; the depth sections of vertical resistivity as a result of the inversion are shown in Figure 6 (upper panel). We then decimate the data and use every other and fourth shot in the inversion i.e. the in-line shot separation is increased from 250 m to 500 and 1000 m, while retaining the same offsets and frequencies as before. The inversion results for the decimated case are shown in Figure 6 middle and lower panels, respectively.

An anisotropic model describes the subsurface resistivity more adequately. The MARE2DEM inversion enables the degree of anisotropy to be controlled via an additional anisotropy regularization term. As part of the data density tests we relaxed the regularization (that penalizes departure from an isotropic model) to enable more anisotropy, if required by the data, in the sub-surface models.

The resistivity model obtained for anisotropy penalty of 0.1 provides the Albatross resistivity anomaly at its correct burial depth (Figure 3, lower panel). However, the recovered

DOI http://dx.doi.org/10.1190/segam2015-5860124.1

Snøhvit anomaly is still inadequate compared to measured resistivity in the well (not shown for brevity). The Snøhvit case illustrates that relaxing the anisotropy penalty improves significantly the recovered resistivity anomaly at the reservoir depth (2.3 km, see Figure 6). Additionally, the recovered resistivity anomalies at Albatross correspond precisely with the fault segments within the structure.

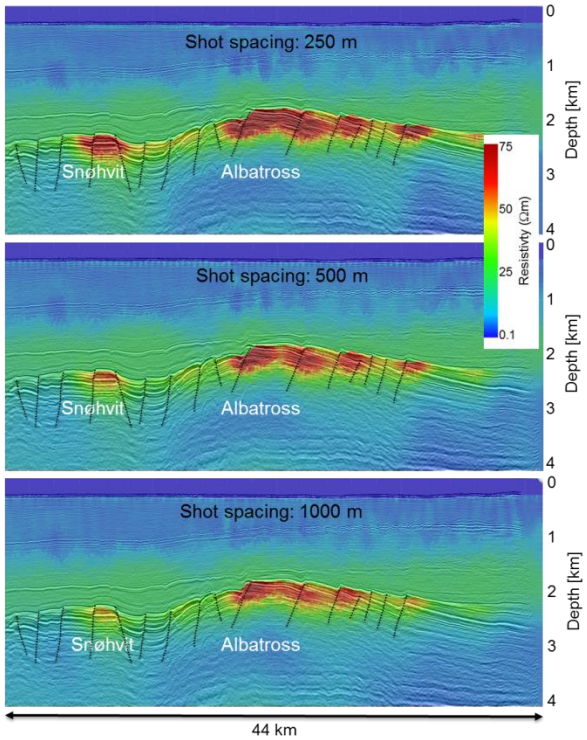

Figure 6: Seismically guided inversion results showing the effects of in-line data density and anisotropy penalty regularization.

For the dense case the vertical resistivity shows a resistive anomaly of 100-125 Ωm at a depth of 2.1 km below the sea level that coincides laterally with the Albatross reservoir location (Figure 6, upper panel). There is also a layer of slightly higher resistivity at 1500 m depth corresponding to a contrasting lithology in the overburden. The horizontal resistivity is somewhat lower throughout the cross section (not shown).

If we now compare the decimated and dense cases we can see that in the decimated case the overburden (at very shallow burial depths) is irregular, spiky and does not look geologically consistent. For example, there are obvious near-surface anomalies that are not present in the dense case. In addition, while there is still a vertical resistivity anomaly coinciding with the Albatross reservoir it is less pronounced compared to the dense-case scenario (Figure 6, lower panel). In particular, we conclude that a 1000 m shot separation is too sparse, whereas 500 m shot separation produce results comparable to those 250 m shot separation. However, lateral smearing is slightly higher in case 500 m separation compared to dense-spaced samples.

The sensitivity to a change in the sub-surface resistivity increases as the data-density increases. The left panel in Figure 7 shows the integrated sensitivity, calculated by summing sensitivity contribution from all frequencies and offsets, for the 250 m shot spacing, whereas the right panel includes the results for a data selection at every fourth shot. Note how the increased sampling increases depth sensitivity, especially in the region of the Albatross discovery.

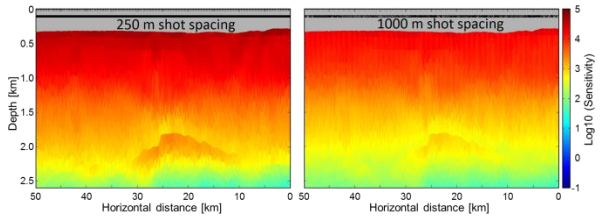

Figure 7: Figure showing sensitivity variation with respect to in-line data density. Note significantly increased sensitivity when using every shot as well as the general trend of decreasing sensitivity with depth.

Summary & Conclusions

Seismically guided anisotropic 2.5D inversion of Towed Streamer EM data significantly improves the lateral and vertical resolution of resistivity anomalies obtained from unconstrained inversion at known HC discoveries of Albatross and Snøhvit areas in the Barents Sea. The resistivity anomalies correspond precisely to the seismically interpreted structures and also to the interpreted well log data at Albatross area. By relaxing the anisotropy penalty in the seismically guided inversion the recovered resistivity of the Albatross structure improves noticeably and corresponds well with individual fault segments within the reservoir. On the other hand a high anisotropy penalty enforces horizontal smoothness and introduces "horizontal banding" as artefacts in the recovered resistivity models.

While guided inversion can improve the resolution we demonstrated that unconstrained inversion can highlight potential prospective structures e.g. a resistivity anomaly that corresponds with a seismically interpreted intra-Cretaceous sand lens. Thus we conclude unconstrained inversion provides "fast track" sub-surface interpretation in frontier exploration and also gives valuable input for parameters selection in a structurally constrained inversion that could be used to further define a prospect, or test hypotheses.

The high data density of a Towed Streamer EM increases the sensitivity to changes in the sub-surface resistivity in comparison to those derived from a coarser data sampling.

Acknowledgements

We thank Petroleum-Geo Services (PGS) for permission to publish this work. We also thank Jens Beenfeldt and Sverre Petlund of PGS Reservoir Services for interpreting the broadband dual-streamer seismic data.

DOI http://dx.doi.org/10.1190/segam2015-5860124.1

EDITED REFERENCES

Note: This reference list is a copyedited version of the reference list submitted by the author. Reference lists for the 2015 SEG Technical Program Expanded Abstracts have been copyedited so that references provided with the online metadata for each paper will achieve a high degree of linking to cited sources that appear on the Web.

REFERENCES

Constable, S. C., R. L. Parker, and C. G. Constable, 1987, Occam's inversion: A practical algorithm for generating smooth models from electromagnetic sounding data: Geophysics, **52**, 289–300. http://dx.doi.org/10.1190/1.1442303.

Du, Z., and S. Hosseinzadeh, 2014, Seismic guided EM inversion in complex geology: Application to the Bressay and Bentley heavy oil discoveries, North Sea: Presented at the 76th Annual International Conference and Exhibition, EAGE. http://dx.doi.org/10.3997/2214-4609.20141250.

Key, K., and J. Ovall, 2011, A parallel goal-oriented adaptive finite element method for 2.5D electromagnetic modeling: Geophysical Journal International, **186**, no. 1, 137–154. http://dx.doi.org/10.1111/j.1365-246X.2011.05025.x.

Løseth, L. O., and B. Ursin, 2007, Electromagnetic fields in planarly layered anisotropic media: Geophysical Journal International, **170**, no. 1, 44–80. http://dx.doi.org/10.1111/j.1365-246X.2007.03390.x.

Mattsson, J., P. Lindqvist, R. Juhasz, and E. Björnemo, 2012, Noise reduction and error analysis for a towed-EM System: 82nd Annual International Meeting, SEG, Expanded Abstracts, http://dx.doi.org/10.1190/segam2012-0439.1.